Chapter 7

Active Stopper

In neutron deficient Sn isotopes where Coulomb excitation experiments are presently not possible due to lack of sufficient beam intensities, decay studies can be performed to obtain the level scheme in these exotic nuclei. At GSI Helmholtzzentrum für Schwerionenforschung radioactive nuclei are produced following relativistic projectile fragmentation and/or fission reactions. By utilizing the magnetic separator Fragment Separator (FRS) [56], specific nuclei of interest can be distinguished from the vast plethora of other secondary products and cleanly transmitted to the final focus, where decay studies may be performed. Such studies make use of the RISING γ-ray array [57] which consists of fifteen, high efficiency seven-element Ge cluster detectors. In order to measure the γ-radiation following alpha and/or beta-decay, the exotic nuclei have to be stopped in an active stopper. It was placed at the final focus and consisted of a series of Double Sided Silicon Strip Detectors (DSSSDs). The DSSSDs were used to determine both the energy and position of the (a) implanted secondary fragment of interest directly from the projectile fragmentation reaction and (b) beta-particle(s) following the subsequent radioactive decay(s) of the often highly exotic nucleus of interest and its daughter decays. The ultimate aim of the device is to correlate beta-decay events to specific exotic radioactive mother nuclei on an event by event basis. In this chapter the development of the active stopper detector is discussed in detail.

7.1 Active Stopper

A new beta counting system has been developed for the RISING (**R**are **I**sotope **S**pectroscopic **IN**vestigation at **G**SI) project [58] to study the β-decay of exotic nuclei produced by projectile fragmentation or fission. This system employs Micron Semiconductor Ltd. [59] Model W1(DS)-1000 DC coupled double-sided silicon strip detectors (DSSSD) with 16 front strips and 16 back strips, each of width 3mm (see fig. 7.1), to detect both fragment implants and their subsequent beta decays.

One of the challenges in designing electronics for the beta counting system is the range of charged particle energies that must be measured. A fast fragment implant will deposit more than 1GeV total energy in the DSSSD, while an emitted beta particle will deposit less

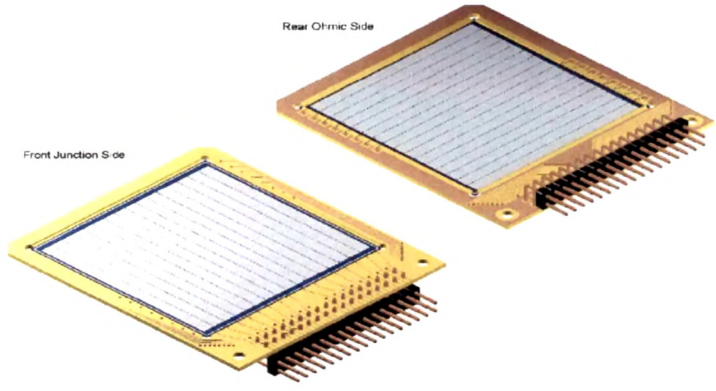

Figure 7.1: Schematic drawing of the W1(DS)-1000 double-sided silicon strip detector (DSSSD) from Micron Semiconductor Ltd [59].

than 1MeV. As can be seen in fig. 7.2, implantation and decay events are directly correlated within each pixel of the detector, providing a measurement of the β-decay time in the seconds range. (Section 7.3 and 7.4) Measurements with Mesytec [60] and Multi Channel Systems [61] electronics will be described and experimental results of a ^{241}Am α-source and ^{207}Bi β-source are discussed. Finally, a measurement with ^{136}Xe ions was performed (Section 7.6) which were implanted in the DSSSD. A summary of the performed RISING experiments is given in Section 7.7.

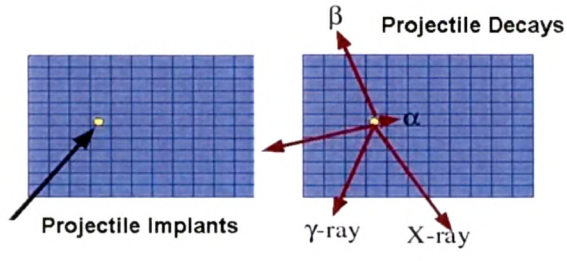

Figure 7.2: Schematic drawing of the position correlation between the projectile implant and the subsequent β-decay measured with the double-sided silicon strip detector (DSSSD).

7.2 GEANT4 Simulation

While this detector thickness provides an efficient implantation of heavy ions, the range of β-particles emitted by the nuclear decays is usually significantly larger than 1mm silicon. This fact results in the probable escape of the particles from the DSSSD before they deposit their full kinetic energy. The deposited energy depends on the path of the electron in the silicon and therefore on the implantation depth. Fig. 7.3 (left) shows the simulated energy

spectrum of the electrons emitted by the β-decay and detected by the DSSSD. A Fermi-Curie initial electron energy distribution with $Q_\beta = 5$MeV was assumed.

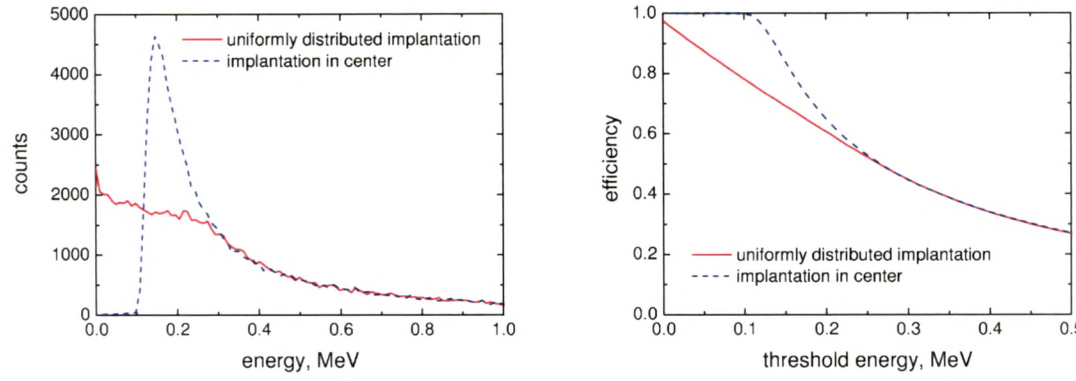

Figure 7.3: Simulated energy spectrum of β-particles emitted from fragments implanted uniformly (solid line) and exactly in the centre (dashed line) of a DSSSD (left). The simulation assumes a Q_β-value of 5MeV and a Fermi-Curie distribution for β-particles. The right figure shows the calculated β-detection efficiency as a function of the DSSSD threshold for the two considered implantation senarios.

For different Q_β- values the displayed energy distribution will only change on the high-energetic side. The Monte-Carlo simulations were performed using GEANT4 simulation toolkit [62] with the 'GEANT4 Low Energy Electromagnetic Physics' package [63]. Two cases of the implantation were considered: uniformly distributed and exact central implantation. In the later case the minimum distance to the surface is 0.5mm which corresponds to the minimum energy which electrons deposit in the crystal. This fact highlights the importance of achieving the low energy threshold at 0.1 MeV as well as the importance of the accurate central implantation. Fig. 7.3 (right) shows the efficiency to detect β-particles in 1mm thick DSSSD in dependence on the energy threshold for the two considered implantation scenarios which is high for a low detection threshold.

7.3 Measurements with *mesytec* Electronics

The mesytec MPR-32 preamplifier was used for the 16 front and 16 back strips of a single DSSSD. Positive and negative charge can be amplified equally. The input connectors are subD 25 female connectors. For the differential outputs twisted pair 34 pin male header connectors are used. For a ^{207}Bi β-source the MPR-32 output signal is displayed in fig. 7.4 with a pulse height of approximately 200mV and a decay time of 30μs. The signal to noise ratio is 10:1.

The mesytec MPR-32 multi-channel preamplifier is available in a linear and logarithmic mode. A typical application of the logarithmic one is decay spectroscopy which allows the

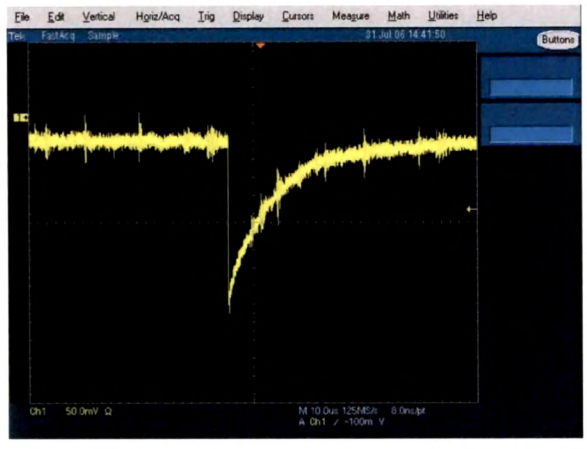

Figure 7.4: Output signal of the MPR-32 preamplifier for a ^{207}Bi β-source (pulse-height 200mV, decay time 30μs)

measurement of both the β-energy (in MeV range) and the implantation of heavy ions (in GeV range) with the silicon detector. The MPR-LOG series provides a linear range, which covers 70% of the total range. The last 30% covers the range up to 3GeV. Fig. 7.5 shows the characteristics of the logarithmic MPR-32 preamplifier which was measured with a research pulser using the correct pulse shape. The pulse height can not be directly related to the implantation energy because of the pulse height defect.

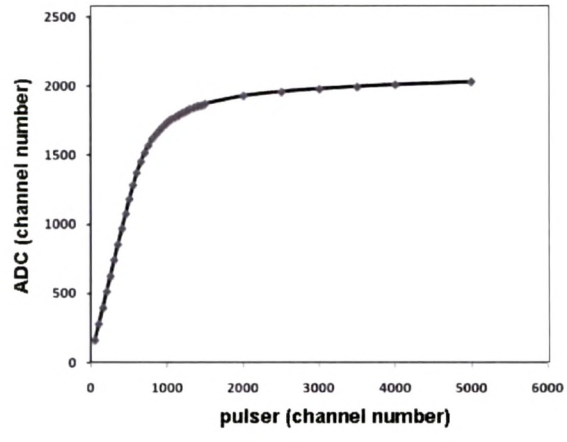

Figure 7.5: The characteristics of the logarithmic MPR-32 preamplifier was measured with a 10 MeV linear range setting and STM-16 spectroscopy amplifiers.

Appendix B.5 shows the maximum incident energy for heavy ions implanted in 0.5mm and 1mm silicon. A switch at the logarithmic MPR-32 preamplifier allows choosing a linear range of 2.5MeV or 10MeV. For the linear MPR-32 preamplifier an amplification range of 5MeV and 25MeV can be chosen.The MPR-32 can easily be combined with two mesytec

STM-16 shaping-/timing filter/ discriminator modules when the differential input version is used. The input resistance must be terminated with 50Ω for the linear MPR-32 and 100Ω for the logarithmic MPR-32. The polarity can be changed with a 4*16 pole connector (inside the case labelled differential input gain 2). Two shaping times of σ=0.4μs/1μs (1.0μs/2.5μs FWHM) can be selected by a jumper (short/long) which is common for all channels. For the following measurements a shaping time of 1μs (FWHM) was selected. The STM-16 can be controlled by a NIM-module MRC-1 which works as a bus master. One mesytec MRC-1 can control 32 various mesytec modules (not only STM-16). It is prepared for the remote control of (i) individual discriminator thresholds (0% to 40% of maximum range, 4V) and (ii) gains (in 16 steps) for pairs of channels. Communication with a control PC is done via RS-232 serial interface.Each analogue signal (34 pin male connector) was fed directly to a CAEN V785AF ADC. The trigger signal of STM-16 was used to produce the ADC gate. Details of the electronic modules and the electronics diagram can be found in Appendix B.1 and B.2. Fig. 7.6 shows the energy spectrum of a ^{207}Bi β-source measured for different discriminator thresholds of the mesytec STM-16 module. The detection limit seems to be at around 150keV.

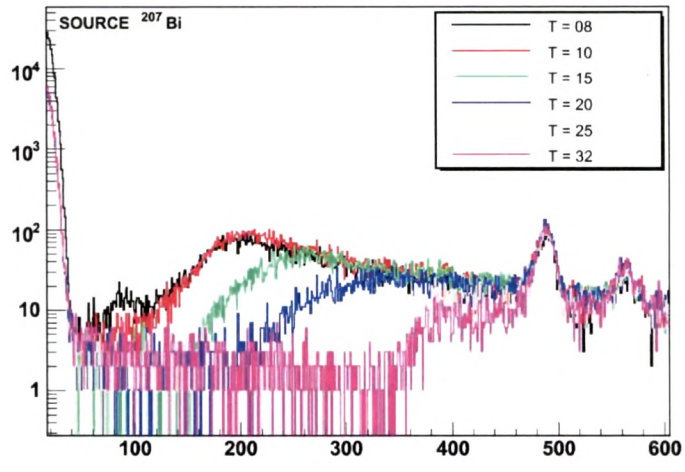

Figure 7.6: Energy spectra of a ^{207}Bi β-source measured for different discriminator thresholds labelled T=8 to T=32 of the Mesytec STM-16 module.

7.3.1 Energy Resolution Measured with α-Particles of a ^{241}Am Source

The energy resolution of the individual strips was measured by a thin ^{241}Am source placed 5cm from the detector's surface in a vacuum vessel, flooding it with α-particles. The range of 5MeV α-particles in silicon is ≈28μm. A Gaussian function was fitted to the 5.486MeV peak. Individual strips displayed energy resolutions of 0.48-0.52 % (front) and 0.51-0.64 % (back) FWHM for the 5.486MeV peak. The edge strips showed a somewhat poorer resolution.

Typical α-energy spectra for individual strips are displayed in fig. 7.7.

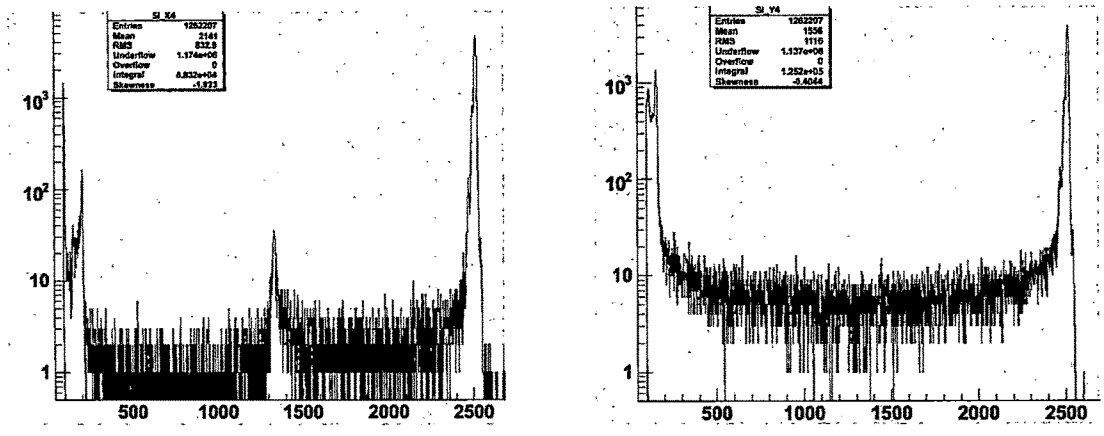

Figure 7.7: Energy spectrum of a ^{241}Am α-source measured with DSSSD-2512-17 front strip X4 (left) and back strip Y4 (right).

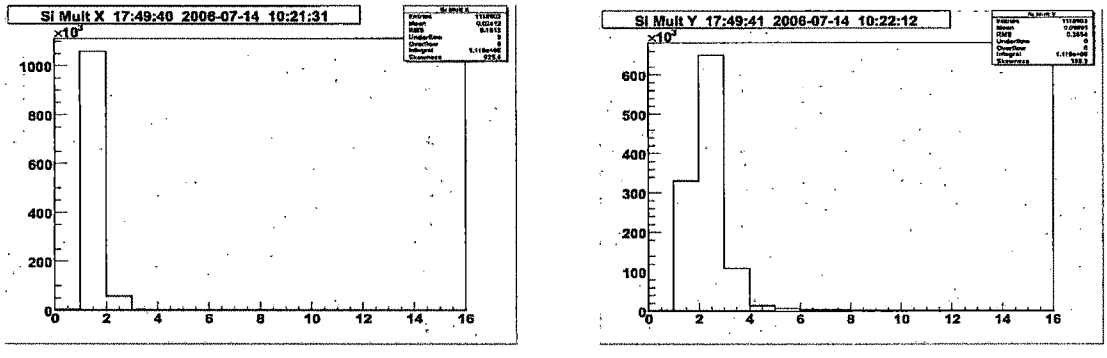

Figure 7.8: Strip multiplicity for front (left) and back (right) side measured for DSSSD-2512-17 at a bias voltage of 40V (detector not fully depleted) for α-particles of a ^{241}Am source.

Neighbouring strips are separated by an insulating gap. It has already been observed by others [64] that a charged particle entering the detector through the gap between the strips induces a reduced pulse height in the front strips in comparison to a particle entering through a strip. This effect is believed to be the result of charge trapping between strips due to the shape of the electric field between the strips. We have also observed this effect (see fig. 7.7). For a fully depleted DSSSD (bias voltage 200 V) the strip multiplicity is close to unity, while the maximum of the strip multiplicity (back side) is shifted to 2 for a detector bias voltage of 40V (fig. 7.8).

The relative efficiency of the strips is roughly constant across the entire detector as it was examined by C. Wrede et al.[64]. Therefore, the distribution of the α-source can be examined with a resolution of 256 pixels. Data were taken under the following condition:

First, the α-source was centred relative to the DSSSD and second, moved to one side of the DSSSD. Fig. 7.9 shows both 3-D histograms of x-position versus y-position. One can clearly see the intensity distribution and the boundaries of the α-source.

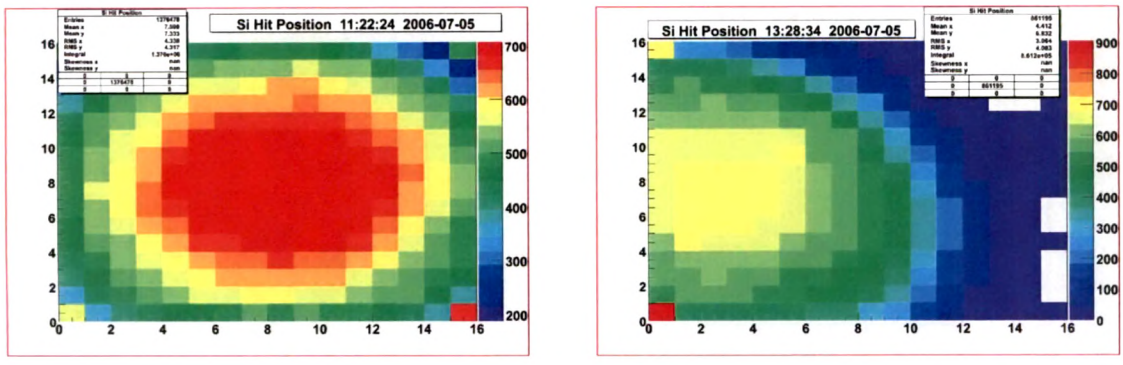

Figure 7.9: 3-D histogram of x-position versus y-position measured for DSSSD-2243-5 with α-particles of a ^{241}Am source. The source is centred (left) and off-centre (right) relative to the DSSSD.

7.3.2 Energy Resolution Measured with Electrons of a ^{207}Bi Source

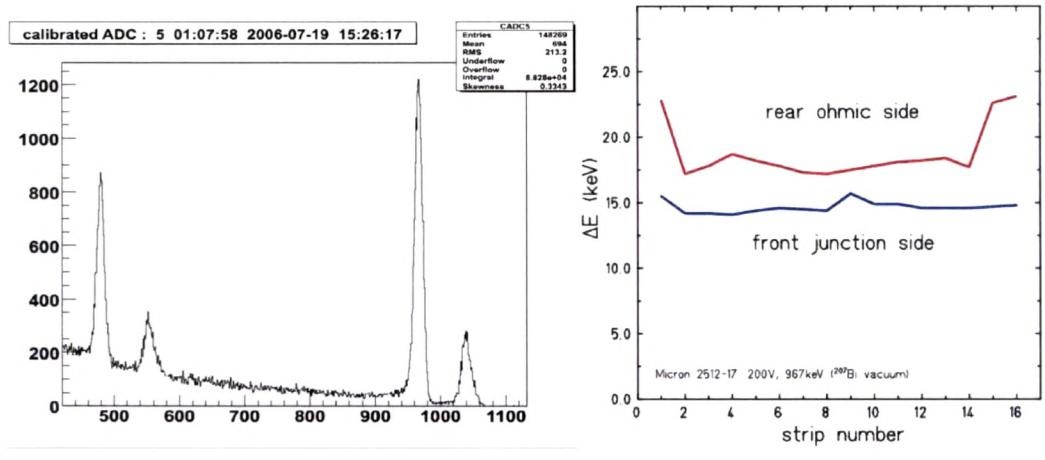

Figure 7.10: The conversion electron spectrum of ^{207}Bi obtained by strip X4 of DSSSD-2512-17. Four peaks at 482keV, 555keV, 976keV and 1049keV are by mono-energetic electrons (left). The energy resolution for the front junction and the rear ohmic side versus the strip number is plotted on the right side.

A ^{207}Bi conversion electron source which emits mono-energetic β-particles was used to calibrate the DSSSD. The ^{207}Bi source was positioned at 5cm from the front face of the detector. The measured electron spectrum for a front strip is shown in Fig. 7.10 (left).

Four peaks (482keV, 555keV, 976keV and 1049keV) are clearly observed, due to K and L conversion electrons of the 570keV and 1060keV transition in ^{207}Pb (see Appendix B.9). The energy resolution of the 976keV line is 14.4keV for this strip . Fig. 7.10 (right) shows an overview of the energy resolution versus the strip number which is better for the front junction side than the rear ohmic side. The comparison between the linear and logarithmic MPR-32 preamplifier shows a slightly poorer energy resolution for the logarithmic one, 19.7keV instead of 15.3keV for a selected front strip (see fig 7.11). However, the logarithmic MPR-32 has the advantage of being able to measure both the heavy-ion implantation as well as the β-particle. All the data discussed so far were obtained for detector tests performed in vacuum. DSSSD tests were also carried out in dry nitrogen. The energy resolutions measured in vacuum and dry nitrogen were the same within the experimental uncertainties. Therefore, the RISING experiments with an active stopper can be performed in dry nitrogen, allowing the use of a detector vessel with thin walls, thereby minimizing the absorption of the emitted γ-rays.

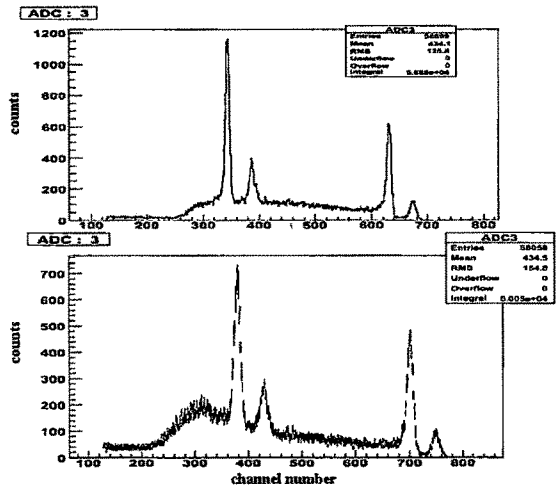

Figure 7.11: The conversion electron spectrum of ^{207}Bi obtained by strip X3 of DSSSD-2243-5 measured with the linear MPR-32 (top) and the logarithmic MPR-32 (bottom). The energy resolution and the signal-to-noise ratio are Δ E=15.3keV and 3.5:1 for the linear MPR-32 and ΔE=19.7keV and 2.6:1 for the logarithmic MPR-32, respectively.

7.4 Measurements with Multi Channel Systems Electronics

At the National Superconducting Cyclotron Laboratory (NSCL) at Michigan State University (MSU) a beta counting system [65] has been developed with different electronics which yields reliable energy information for both implants and decays. The DSSSD signals are first processed by two 16-channel charge sensitive preamplifier modules CPA-16 supplied by *Multi Channel Systems* [61]. These modules contain precision pre- and shaping amplifier electronics and provide both high gain (2V/pC) and low gain (0.1V/pC) analogue outputs. One module was specified to have inverted output signals, and the other one non-inverted, so that the processed outputs from both the front and backsides of the DSSSD share the same polarity. For a ^{207}Bi β-source the CPA-16 output signal is displayed in fig. 7.12 with a pulse height of approximately 200 mV and a width of about 1μs.

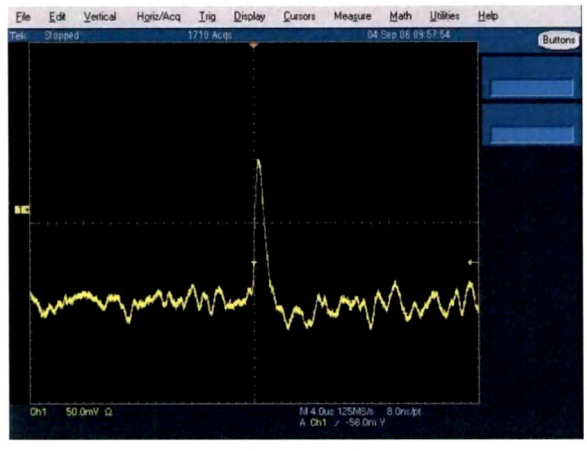

Figure 7.12: Output signal of the CPA-16 preamplifier for a ^{207}Bi β-source.

Therefore, a high counting rate of at least 100 kHz can be applied without pulse pile-up. The signal to noise ratio is 7:1. As a result, the low gain signals, which provide the fast fragment implantation energy information, can be sent directly to *CAEN* V785AF ADC with no further shaping. As the high gain signals carry information from low-energy beta decay events, they require further processing. This is accomplished at MSU using Pico Systems [66] 16-channel shaper/discriminator modules in *CAMAC*. The shaper output of the Pico Systems module is sent directly to an ADC while each discriminator output is combined in a logical OR gate to provide the master trigger. Since Pico Systems modules were not available at GSI, *ORTEC* 572 and 16-channel *CAEN* N568BC amplifiers were used for further shaping the high gain CPA-16 output signals. Details of the electronic modules and the electronics diagram can be found in Appendix B.3 and B.4.

7.4.1 Energy Resolution Measured with β-Particles of a ^{207}Bi Source

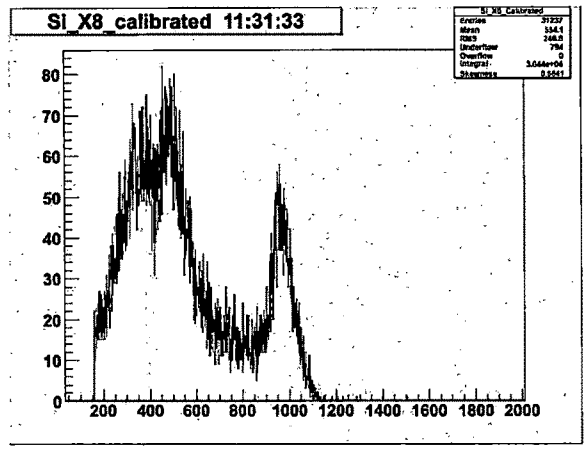

Figure 7.13: The conversion electron spectrum of ^{207}Bi obtained by a strip of DSSSD-2243-5. Two peaks at 482keV and 976keV are by mono-energetic electrons. The high gain output signal of the CPA-16 preamplifier was sent directly to the ADC.

A ^{207}Bi conversion electron source was used to measure the electron spectrum for one representative strip of DSSSD-2243-5 (fig. 7.13). The β-source was also positioned about 5cm from the front face of the detector. Three different measurements were performed: (i) the high gain output signal of the CPA-16 preamplifier was sent directly to the ADC, (ii) it was additionally amplified with *ORTEC* 572 using shaping times of 0.5s, 1.0s and 2.0s, respectively and (iii) with *CAEN* N568BC with shaping time 2.0s before sending it to the ADC.

Fig. 7.13 shows the conversion electron spectrum of ^{207}Bi without further amplification. Only two peaks (482keV and 976keV) are clearly seen and are due to K conversion electrons of the 570keV and 1060keV transition in ^{207}Pb. The energy resolution of the 976keV line is 100keV. The detection limit seems to be at around 300keV. The measured energy resolutions with ORTEC 572 and CAEN N568BC are summarized in the table 7.1 below.

Shaping time [μs]	ORTEC 572	CAEN N568C
0.5	122keV	
1.0	112keV	
2.0	103keV	113keV

Table 7.1: The measured energy resolutions with ORTEC 572 and CAEN N568BC

In conclusion, for the DSSSD an energy resolution of 15keV and an energy threshold of 150keV have been measured for the mesytec electronic which compares to a FWHM of 100keV and a threshold of 300keV for Multi Channel Systems electronics.

7.5 Chamber for the RISING Active Stopper

After the decision to operate the DSSSD in dry nitrogen, γ-transmission measurements were performed with ^{57}Co (E_γ=0.122, 0.136MeV) and ^{60}Co (E_γ=1.173, 1.332MeV) sources. Different aluminium plates varying between 1mm and 5mm as well as printed circuit board material Pertinax (phenolic-formaldehyd cellulose-paper PF CP 2061) of 6mm thickness were irradiated and the none absorbed γ-rays were detected in a Geiger-Müller counter. The ratio of the γ-transmission of aluminium and Pertinax is plotted in fig. 7.14 as a function of the Al-layer thickness.

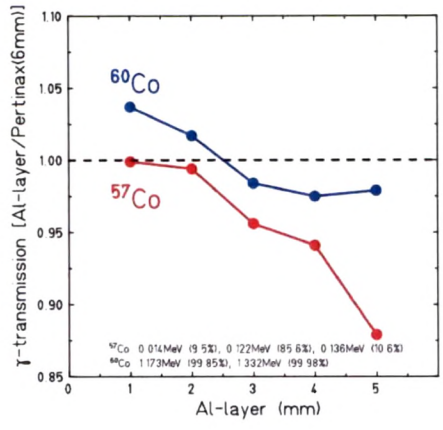

Figure 7.14: The ratio of the γ-transmission of aluminium and the printed circuit board material Pertinax is plotted as a function of the Al-layer. The γ-transmission of both materials is equal for a thickness of 2mm aluminium

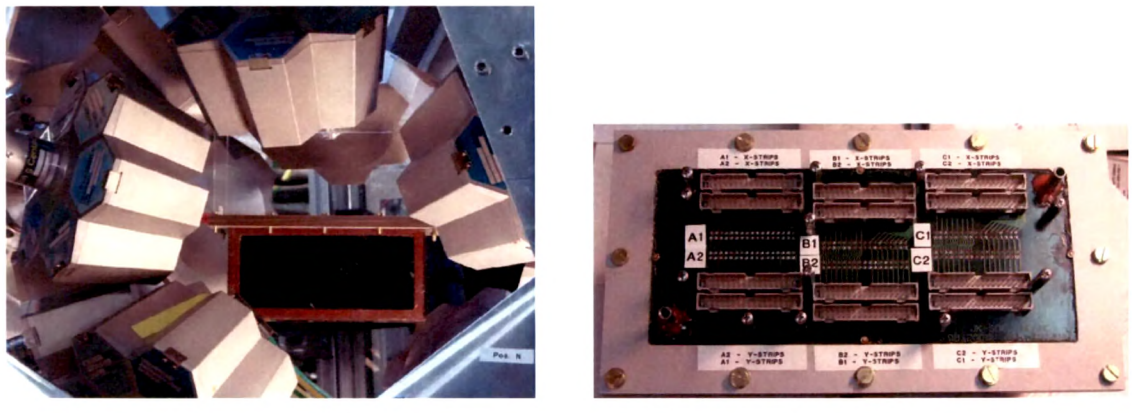

Figure 7.15: The Cluster array of the stopped beam RISING experiments with the active stopper vessel made out of Pertinax (left) and the top cover of the active stopper chamber with the cable connectors (right) for six DSSSD arranged in two rows.

The γ-transmission of both materials is equal for a thickness of 2mm aluminium. Since

the chamber of the active stopper can be produced with Pertinax of 2mm thickness, the aluminium equivalent is 0.7mm. Fig. 7.15 shows the active stopper chamber produced out of 2mm Pertinax with an entrance and exit window covered by a thin black Pocalon C foil (20μm). The top cover of the chamber shows the cable connectors for six DSSD which can be arranged in two rows.

A ^{207}Bi conversion electron source was mounted in front of the new Pertinax chamber and the electron spectrum was measured for DSSSD-2243-2. The mesytec electronic was used to obtain the energy resolution which yields an average value of 15.1keV for the front junction side (X-strips).

7.6 Implantation Measurement with a ^{136}Xe Beam

A test measurement has been performed with the RISING set-up (fig. 7.16) in the final focal plane area (S4) of the fragment separator (FRS) at GSI to investigate the heavy ion implantation in the double-sided Si-strip detector. A primary beam of ^{136}Xe with 400AMeV was used to be slowed down in the S4-degrader and finally implanted in the silicon detector. The active stopper vessel for the DSSSD is depicted in fig. 7.15 surrounded by the Cluster array of the stopped beam RISING experiments.

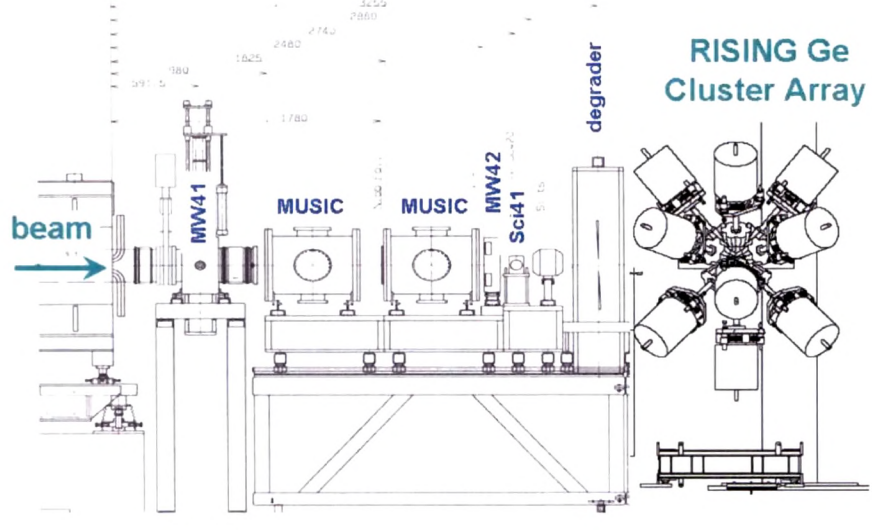

Figure 7.16: Schematic layout of the RISING set-up at the final focal plane area (S4) of the FRagment Separator (FRS) at GSI. The beam diagnostic elements consist of two multiwire detectors (MW41 and MW42), two ionisation chambers (MUSIC) and two scintillation detectors (Sc21 and Sc41). The degrader allows an accurate implantation of the heavy ions in the active stopper, which is surrounded by Ge-Cluster detectors for γ-ray measurement.

Two measurements were carried out with the linear and logarithmic MPR-32 preamplifiers. They were placed 30cm away from the DSSSD and combined with two mesytec

STM-16 shaping-/timing filter/ discriminator modules (at a distance of 10m). The STM-16 units were operated with a gain-value of 1 and a threshold of 20. For the planned decay experiment the optimal settings are a gain-factor of 2 and the threshold as low as possible (e.g. 2-3) to reach the highest efficiency for electron detection. The scintillation detector Sc41 served as a trigger for the measurement.

7.6.1 Results with the Linear MPR-32 *mesytec* Preamplifier

The linear MPR-32 preamplifier is well suited for the electron measurement (MeV range), however, for the implantation of heavy ions (GeV range) the output signals saturate. A collection of the measured preamplifier signals can be found in Appendix B.6. The measured energy spectra (10MeV range setting) obtained by x-strips (front junction) of DSSSD-2243-5 are shown in fig. 7.17 for the implantation of ^{136}Xe ions.

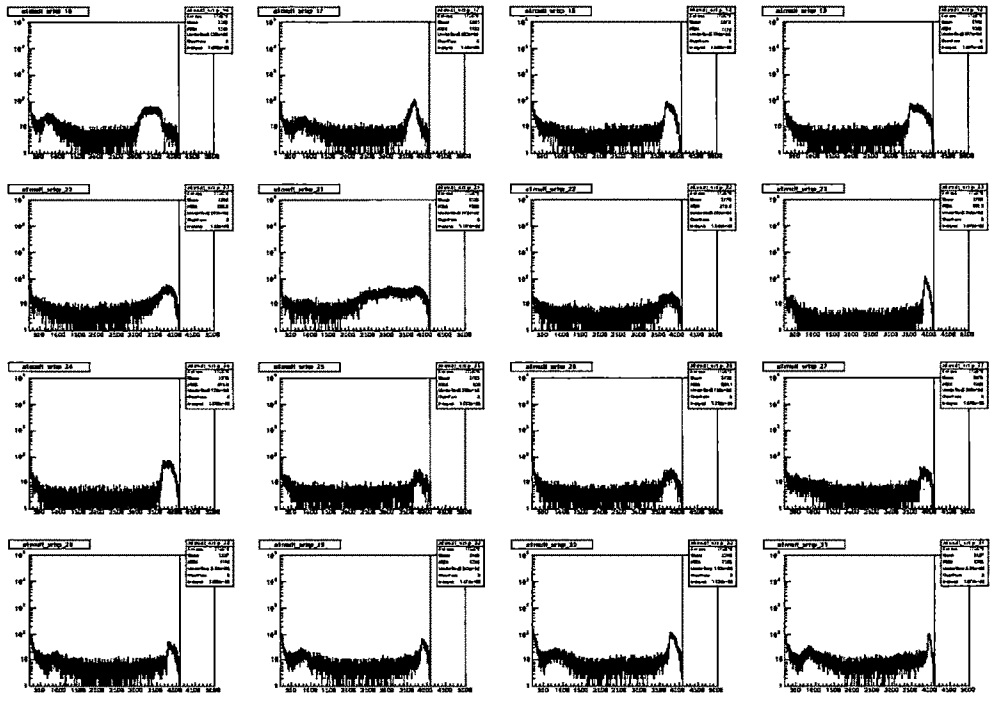

Figure 7.17: Measured energy spectra (10MeV range of the linear MPR-32 preamplifier) obtained by x-strips (front junction) of DSSSD-2243-5 for the implantation of ^{136}Xe ions.

They show the low energetic part of the implantation caused by light charged particles and atomic X-rays. In most cases all the strips of the DSSSD fire, since no condition is set on the implantation of the heavy ions. Fig. 7.18 shows the x-strip multiplicity distributions for different energy thresholds. If one takes only the overflow data of the energy spectra

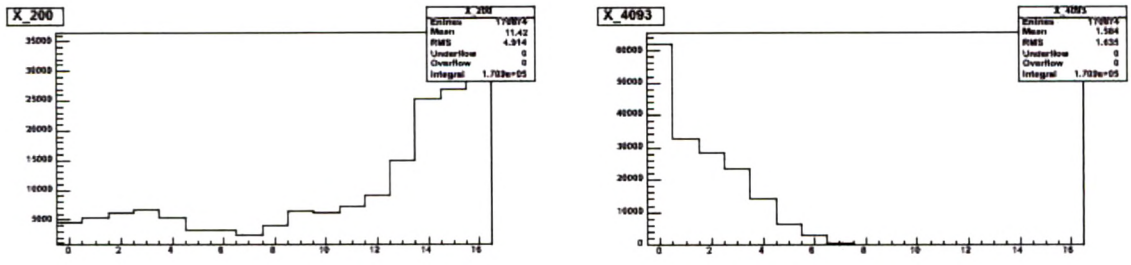

Figure 7.18: Multiplicity distributions measured by x-strips of DSSSD-2243-5 for different energy thresholds. For a very low threshold (channel number 200) almost all x-strips are firing, while for the overflow (>10MeV) data the hit probability is very low, as expected for the implantation of ^{136}Xe ions.

(>10MeV), the multiplicity spectrum is localized at small values, which is expected for the implantation. For multiplicity one on each side of DSSSD the position is uniquely determined, while for higher multiplicities the centroid has to be determined.

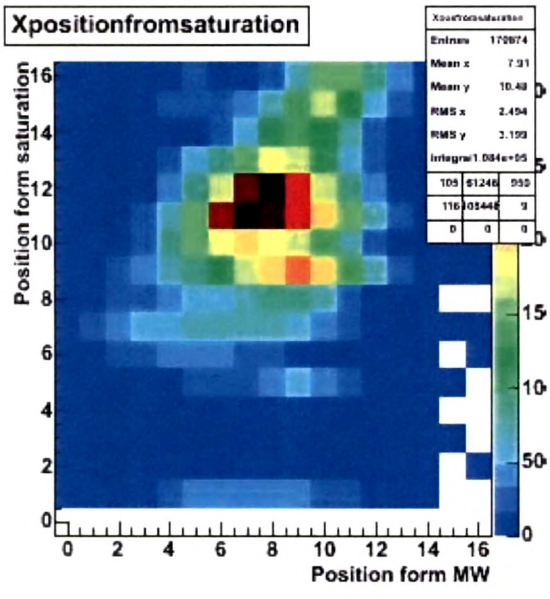

Figure 7.19: Position correlation between the multiwire detector MW and the DSSSD-2243-5. In case of the DSSSD the position of the implanted ^{136}Xe ion was determined from the overflow data, when a linear MPR-32 preamplifier was used.

In case of the linear MPR-32 preamplifier each strip has the same weight for this calculation, since the individual strip energies are not measured. Based on the overflow data, a position correlation between the DSSSD and the multiwire detector MW was determined which is displayed in fig. 7.19.

The correlation shows that the data measured with the linear MPR-32 preamplifier can be used for a position determination of the implanted ^{136}Xe ions. In conclusion, the overflow data of the DSSSD allow a zero order position determination of the heavy ion implantation.

7.6.2 Results with the Logarithmic MPR-32 *mesytec* Preamplifier

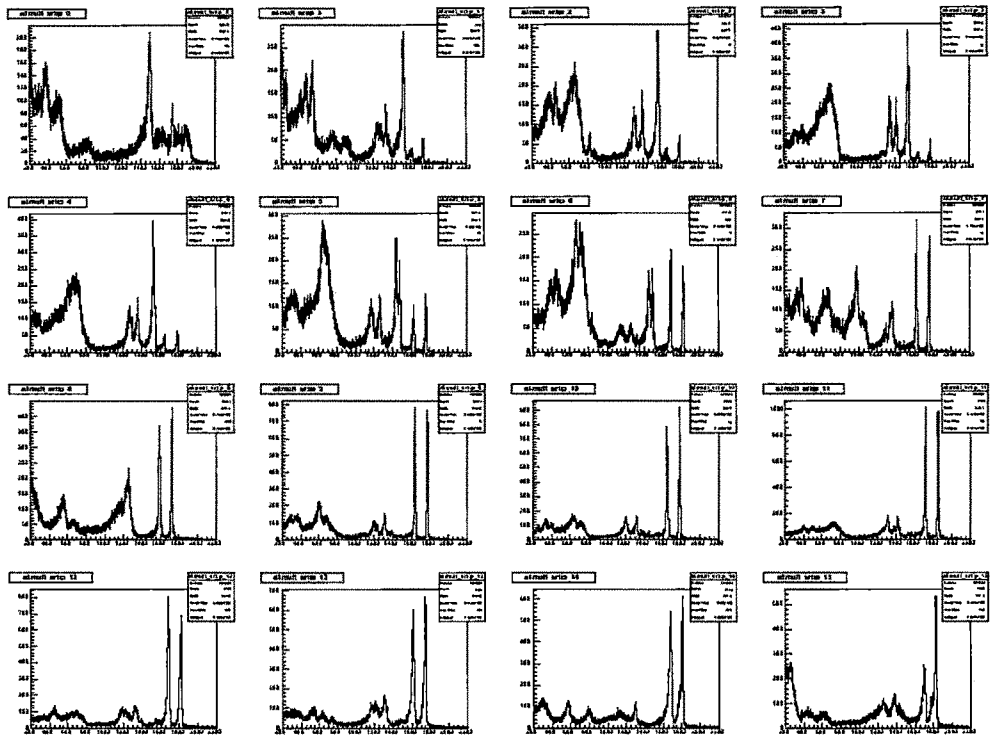

Figure 7.20: Measured energy spectra (10MeV range for the linear part of the logarithmic MPR-32 preamplifier) obtained by x-strips (front junction) of DSSSD-2243-5 for the implantation of ^{136}Xe ions. The double hump structure is related to the stopping of the heavy ions.

The logarithmic MPR-32 preamplifier is well suited for both the electron measurement (MeV range) and the heavy ion implantation (GeV range). A collection of the measured preamplifier (logarithmic MPR-32) signals and amplifier (STM-16) signals can be found in Appendix B.7 and B.8, respectively. The measured energy spectra (10MeV range setting for the linear part of the logarithmic preamplifier) obtained by x-strips (front junction) of DSSSD-2243-5 are shown in fig. 7.20 for the implantation of ^{136}Xe ions. They show a similar distribution at low energy (<10MeV), as compared to the linear MPR-32, and a pronounced double hump structure in the logarithmic part of the spectrum.

The double hump structure, which relates to the implantation of the ^{136}Xe ions, was aligned for each strip and the strip multiplicity for the highest peak was determined. Fig. 7.21 shows the multiplicity distribution for the heavy ion implantation. In most cases only one or two strips on the x- and y-side of DSSSD were activated. It turns out that the highest peak of the double hump structure is related to the implantation, while the second highest peak is interpreted as a cross talk event with the neighbouring strip. The result of the double hump analysis is also displayed in fig. 7.21 showing the hit pattern of the multiplicity 2 events. In 90% of all cases the second highest peak is in a neighbouring strip.

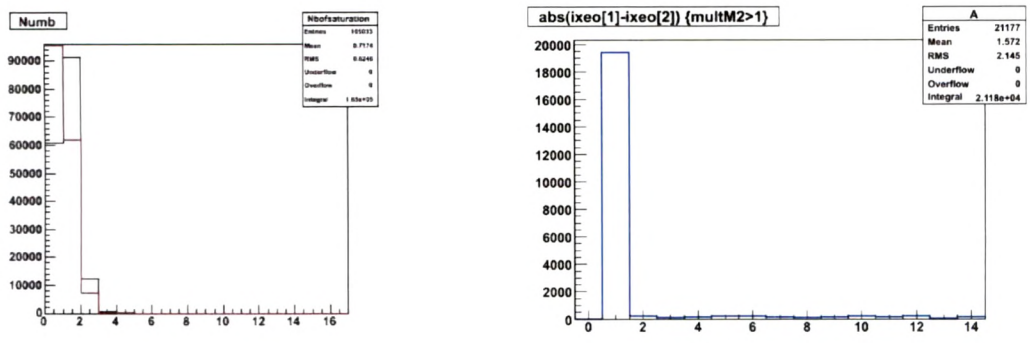

Figure 7.21: Multiplicity distribution for the higher peak of the double hump structure (left). The black distribution shows the result for all x-strips of DSSSD-2243-5, while for the red one strip=1 was removed, which seemed to be very noisy. The right diagram shows the hit pattern relative to the strip with the highest peak for multiplicity 2 events. In 90% of all cases the second highest peak is in a neighbouring strip.

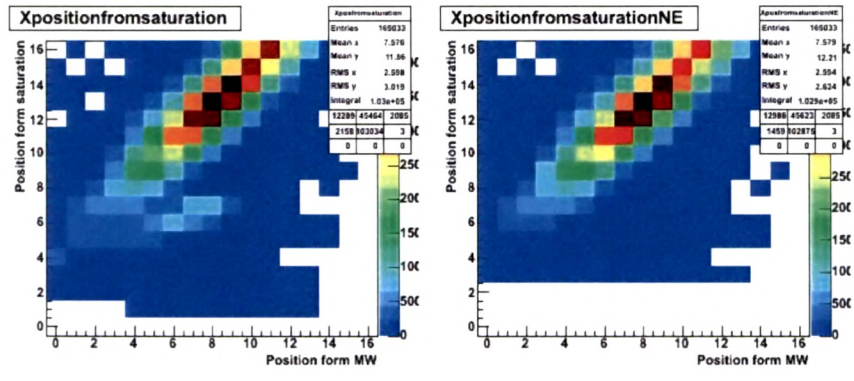

Figure 7.22: Position correlation between the multiwire detector MW and the DSSSD-2243-5. In case of the DSSSD the position of the implanted ^{136}Xe ion was determined from the mean of highest peak, when a logarithmic MPR-32 preamplifier was used. The left correlation includes all strips, while for the right one a single noisy strip was removed.

In case of the logarithmic MPR-32 preamplifier the mean of the highest peak of the

double hump structure was used for the position determination. In fig. 7.22 the position correlation between the DSSSD and the multiwire detector MW is displayed. It shows a strong correlation but also an offset since the DSSSD was not accurately centred in the frame of the FRS. In conclusion, the logarithmic MPR-32 preamplifier is recommended to be used for the active stopper measurements.

7.7 Experiments with Active Stopper

The following RISING experiments have made use of the newly developed active stopper. They will be briefly summarized in the following:

1. **P. H. Regan** *et al.* **-First results with the RISING active stopper [67].**
   This paper outlines some of the physics opportunities available with the GSI RISING active stopper and presents preliminary results from an experiment aimed at performing beta-delayed gamma-ray spectroscopic studies in heavy-neutron-rich nuclei produced following the projectile fragmentation of a 1 GeV per nucleon ^{208}Pb primary beam. The energy response of the silicon active stopping detector for both heavy secondary fragments and beta-particles is demonstrated and preliminary results on the decays of neutron-rich Tantalum (Ta) to Tungsten (W) isotopes are presented as examples of the potential of this technique to allow new structural studies in hitherto experimentally unreachable heavy, neutron-rich nuclei. The resulting spectral information inferred from excited states in the tungsten daughter nuclei are compared with results from axially symmetric HartreeFock calculations of the nuclear shape and suggest a change in ground state structure for the N = 116 isotone ^{190}W compared to the lighter isotopes of this element.

2. **N. Alkhomashi** *et al.* **- β^--delayed spectroscopy of neutron-rich tantalum nuclei: Shape evolution in neutron-rich tungsten isotopes [68].**
   The low-lying structure of ^{188,190,192}W has been studied following β decays of the neutron-rich mother nuclei ^{188,190,192}Ta produced following the projectile fragmentation of a 1-GeV-per-nucleon ^{208}Pb primary beam on a natural beryllium target at the GSI Fragment Separator. The β-decay half-lives of ^{188}Ta, ^{190}Ta, and ^{192}Ta have been measured, with γ -ray decays of low-lying states in their respective W daughter nuclei, using heavy-ion β-γ correlations and a position-sensitive silicon detector setup. The data provide information on the low-lying excited states in ^{188}W, ^{190}W, and ^{192}W, which highlight a change in nuclear shape at ^{190}W compared with that of lighter W isotopes. This evolution of ground-state structure along the W isotopic chain is discussed as evidence for a possible proton subshell effect for the A $\sim$190 region and is consistent with maximization of the γ-softness of the nuclear potential around N $\sim$116.

3. **Zs.Podolyák** *et al.* **- Proton-hole excitation in the closed shell nucleus ^{205}Au [69].**
The neutron-rich N = 126 nucleus ^{205}Au has been populated following the relativistic energy projectile fragmentation of E/A = 1 GeV ^{208}Pb, and studied via charged-particle decay spectroscopy. An internal decay with a transition energy of 907(5) keV and a half-life of $T_{\frac{1}{2}}$= 6(2) s has been identified through the observation of the corresponding K and L internal conversion electron lines (see fig. 7.23). The 907 keV energy level corresponds to the $\pi\ h^{-1}_{11/2}$ proton-hole state and decays both internally into the $\pi\ d^{-1}_{3/2}$ ground-state and via β-decay into ^{205}Hg. The obtained data provides information on the evolution of single-proton hole energies which are vital inputs of shell model descriptions for nuclei around the $^{208}_{82}Pb^{126}$ doubly magic core.

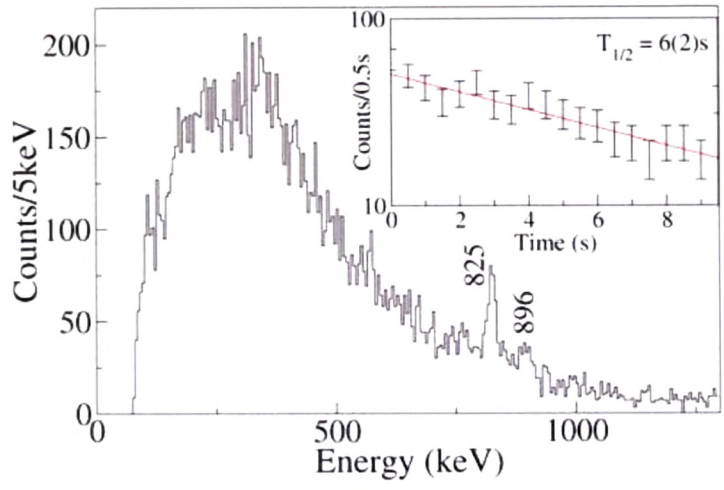

Figure 7.23: Delayed charged particle spectrum associated to ^{205}Au. In addition to the continuous energy of the β-decay, two peaks are observed. These are interpreted as K and L internal conversion electron peaks corresponding to a 907(5) keV transi-tion.

4. **P.H.Regan** *et al.* **- New insights into the structure of exotic nuclei using the RISING active stopper [70].**
This conference paper outlines the operation and some of the preliminary physics results using the GSI RISING active stopper. Data are presented from an experiment using combined isomer and beta-delayed gamma-ray spectroscopy to study low-lying spectral and decay properties of heavy-neutron-rich nuclei around A$\sim$190 produced following the relativistic projectile fragmentation of ^{208}Pb primary beam. The response of the RISING active stopper detector is demonstrated for both the implantation of heavy secondary fragments and in-situ decay of beta-particles. Beta-delayed gamma-ray spectroscopy following decays of the neutron- rich ^{194}Re isotopes is presented to demonstrate the experimental performance of the set-up. The resulting information

inferred from excited states in the W and Os daughter nuclei are compared with results from Skyrme Hartree-Fock predictions of the evolution of nuclear shape.

5. **A.I. Morales *et al.* - β-delayed γ-ray spectroscopy of heavy neutron rich nuclei south of lead [71].**
Relativistic projectile fragmentation of a ^{208}Pb primary beam has been used to produce neutron-rich nuclei with proton-holes relative to the Z = 82 shell closure, i.e., south of Pb. β-delayed γ-ray spectroscopy allows to investigate the structural properties of such nuclei with A 195 205. The current work presents transitions de-exciting excited states in ^{204}Au, which are the first spectroscopic information on this N = 125 isotone.